



# Mineralogy and Pore Structure of Marine–Continental Transitional Shale: A Case Study of the Upper Carboniferous Keluke Formation in the Eastern Qaidam Basin, China

Yingchun Guo<sup>1,2,3</sup>, Xinxin Fang<sup>1,3\*</sup>, Haifeng Wang<sup>4</sup> and Na Wang<sup>4</sup>

<sup>1</sup>Institute of Geomechanics, Chinese Academy of Geological Sciences, Beijing, China, <sup>2</sup>Hubei Key Laboratory of Marine Geological Resources, China University of Geosciences, Wuhan, China, <sup>3</sup>Key Laboratory of Paleomagnetism and Tectonic Reconstruction, Ministry of Natural Resources, Beijing, China, <sup>4</sup>Exploration and Development Research Institute of Qinghai Oilfield Company, Gansu Dunhuang, China

## OPEN ACCESS

### Edited by:

Dongdong Liu,  
China University of Petroleum, China

### Reviewed by:

Tao Hu,  
China University of Petroleum, China  
Pengwei Wang,  
SINOPEC Petroleum Exploration and  
Production Research Institute, China

### \*Correspondence:

Xinxin Fang  
38530324@qq.com

### Specialty section:

This article was submitted to  
Economic Geology,  
a section of the journal  
Frontiers in Earth Science

**Received:** 30 November 2021

**Accepted:** 27 December 2021

**Published:** 09 February 2022

### Citation:

Guo Y, Fang X, Wang H and Wang N  
(2022) Mineralogy and Pore Structure  
of Marine–Continental Transitional  
Shale: A Case Study of the Upper  
Carboniferous Keluke Formation in the  
Eastern Qaidam Basin, China.  
*Front. Earth Sci.* 9:825173.  
doi: 10.3389/feart.2021.825173

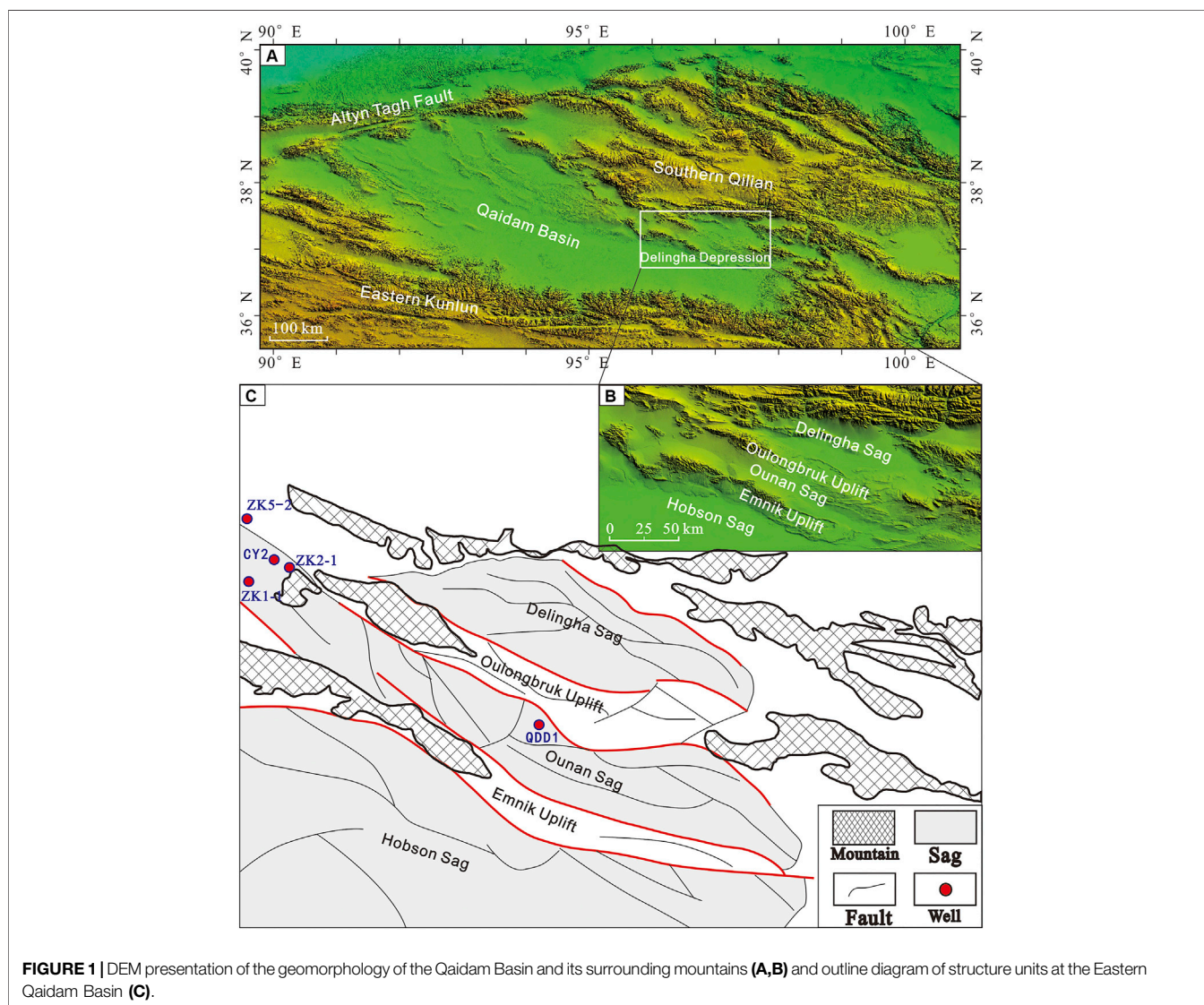
Organic-rich shale and associated fine-grained sedimentary rocks of marine-continental transitional facies were well developed in the Upper Carboniferous Keluke Formation in the Eastern Qaidam Basin, which is expected to be a set of potential shale gas exploration and development target. Mineralogy and pore structure of marine-continental transitional shale were investigated systematically based on thin-section identification, X-ray diffraction (XRD), helium porosity test and pressure-pulse permeability measurement, scanning electron microscopy (QEMSCAN), field emission scanning electron microscopy (FESEM), and high-pressure mercury injection (MICP) and nitrogen adsorption. Thin section, XRD, and QEMSCAN data suggest that marine–continental transitional shale has complex mineral compositions, resulting in mixed rocks and mixed sequences. FE-SEM images show that interparticle and intercrystalline pores are popular in the Keluke Shales, with minor dissolution pores and microfractures. No secondary organic matter pores occur in the Keluke Shales because organic macerals are dominated by vitrinite and inertinite, where only primary pores can be found among organic matter frameworks. MICP and nitrogen adsorption indicate that pore size distributions follow a bimodal pattern and proportions of micro-scale pores and macro-scale pores increase in an order: bioclastic limestone, argillaceous bioclastic limestone, silty mudstone, argillaceous siltstone. The differences in pore structure are caused by sedimentary facies and associated mineralogy and diagenesis. This study can provide a crucial theoretical guidance for sweet spots determination and deep understanding of transitional shale gas potential.

**Keywords:** pore type, pore size distribution, marine-continental transitional shale, mineral composition, Qaidam Basin

## INTRODUCTION

Organic-rich shales are primary targets for unconventional oil and gas exploration and development around the world (Jarvie et al., 2007; EIA, 2013; Zou et al., 2019). These shales are classified into three types based on origins, including marine shales, marine–continental transitional shales, and continental shales (Zou et al., 2019; Dong et al., 2021). Significant attention has been attracted by marine and continental shales in recent years, where considerable progress has been achieved (Curtis, 2002; Dai et al., 2016; Sweere et al., 2016; Li et al., 2017; Zou et al., 2019; Liu et al., 2021). Comparatively, marine–continental transitional shale is poorly investigated, which requires further and comprehensive study (Chalmers et al., 2012; Zhang et al., 2021). Petrological and geochemical properties of shales vary greatly with deposition environment (Zou et al., 2019). Furthermore, transitional shales are characterized by a frequent lithology alternation in vertical because of rapid variation in water depth during deposition.

Transitional shales are commonly small in thickness and are interbedded with tight sandstone, limestone, and coal, resulting in a unique pore structure (Gentzis, 2013; Yang et al., 2017; Qi et al., 2020). Marine-continental transitional sedimentary facies can be divided into various sub-facies (Galloway, 1998; Boggs, 2012; Harraz, 2013). Dong et al. (2021) divide it into five sub-facies: delta facies, estuarine facies, lagoon facies, barrier island facies, and tidal flat facies. Current research on transitional shales in China mainly focuses on Carboniferous-Permian in the Ordos Basin and Yangtze area, which are dominated by delta facies and shallow sea shelf facies, respectively (Yan et al., 2015; Zhang et al., 2015; Guo et al., 2018; Kuang et al., 2020). Organic-rich shales and associated fine-grained transitional deposits in the Upper Carboniferous Keluke Formation in the Eastern Qaidam Basin were primarily developed in the tidal flat and lagoon facies (Zhang et al., 2016), forming frequently mixed carbonate-siliciclastic sequences (Wei et al., 2018). Currently, mixed carbonate-siliciclastic fine-grained rocks in continental and



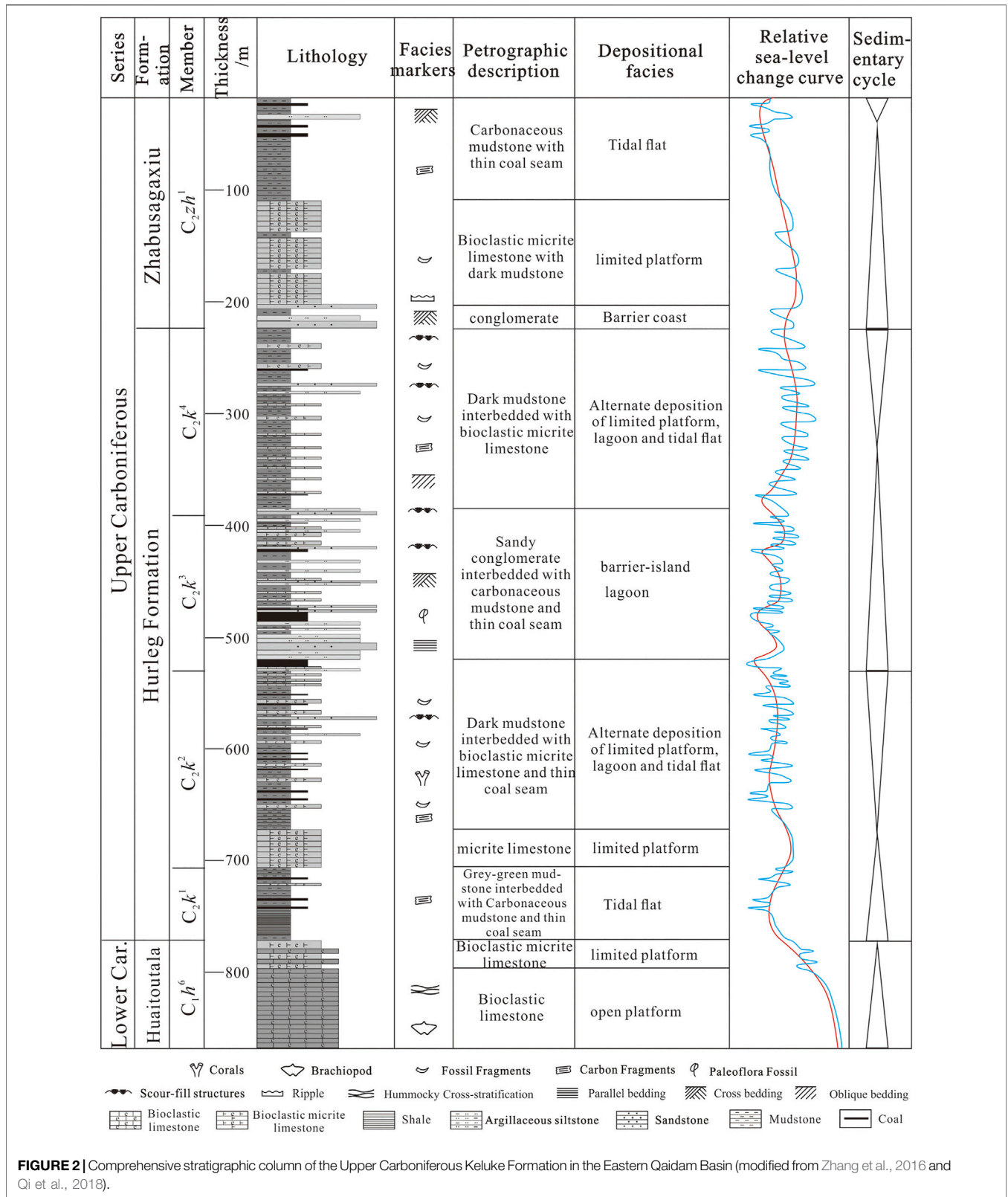


**FIGURE 2** | Comprehensive stratigraphic column of the Upper Carboniferous Keluke Formation in the Eastern Qaidam Basin (modified from Zhang et al., 2016 and Qi et al., 2018).

marine facies and their roles in petroleum accumulation have been widely investigated (Zecchin and Catuneanu, 2017; Abdel-Fattah et al., 2018; Zhang et al., 2018), whereas forming

mechanism of high-quality reservoirs in transitional fine-grained rocks is poorly understood (Ng et al., 2019; Silva et al., 2021).

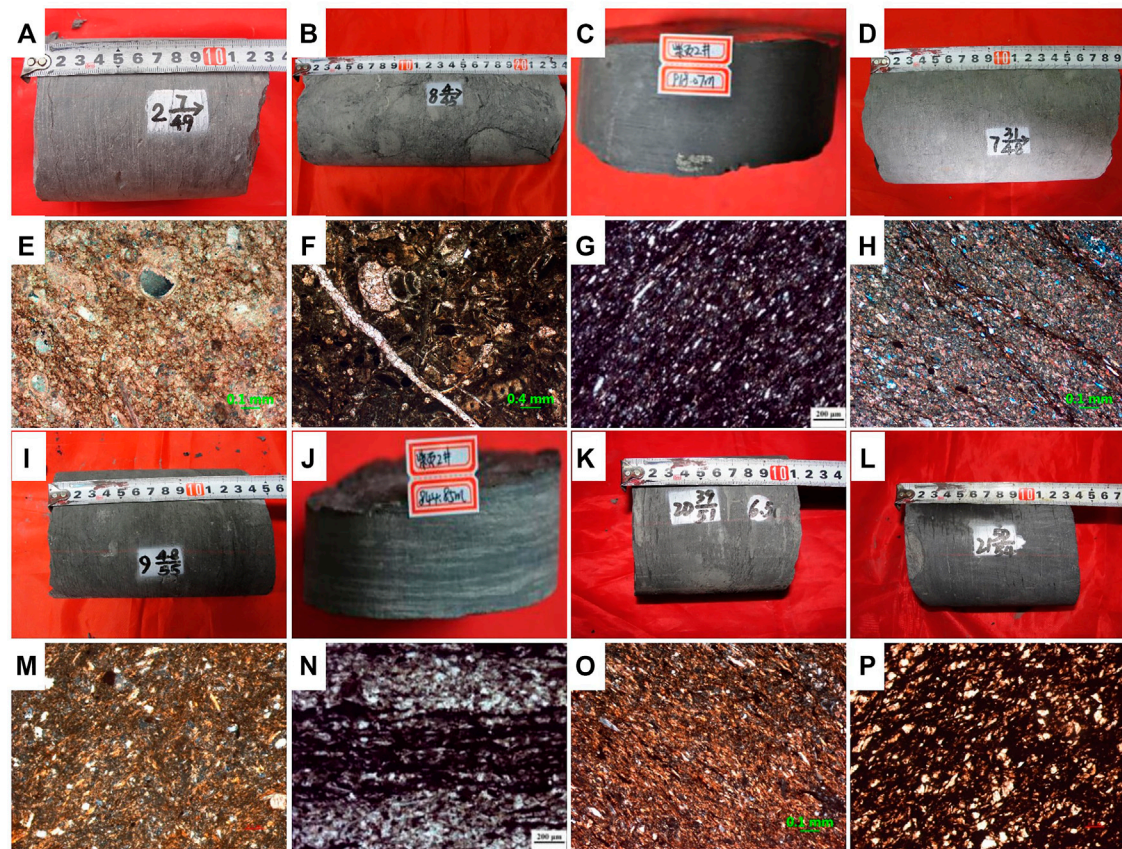


**FIGURE 3** | Various lithologies of transitional shales in the Upper Carboniferous Keluke Formation. **(A,E)**: Limestone, dominated by recrystallized calcite with minor bioclastic. **(B,F)**: Argillaceous bioclastic limestone. **(C,G)**: Black laminated argillaceous siltstone, pyrite. **(D,H)**: Calcareous mudstone. **(I,M)**: Gray black silty mudstone. **(J,N)**: Black striped argillaceous siltstone. **(K,O)**: Mudstone. **(L,P)**: Gray black silty carbonaceous mudstone.

Previous researchers have evaluated shale gas prospects of the Carboniferous sequences in the Eastern Qaidam Basin based on outcrops and shallow well data, which reported that the Keluke Formation had good shale gas enrichment conditions (Yang et al., 2014; Liu et al., 2016). Some researchers have identified lithofacies and reservoir development in the Keluke Shales in the eastern Qaidam Basin using outcrops (Li et al., 2015; Chen et al., 2016a; Zhang et al., 2016; Liu et al., 2020). However, pore structures and their controllers in the Keluke fine-grained reservoirs (shale, tight sandstone, tight mixed rocks, etc.) are not well understood. More accurately, fine-grained deposits with grain size less than 62.5  $\mu\text{m}$  can be defined as shale, which has nothing to do with mineral composition and lithofacies (Jiang and Tang, 2017). The CY2 well in the SHG area in the Eastern Qaidam Basin exhibits good gas show from the Carboniferous Keluke transitional organic-rich shales (Cao et al., 2016). Hydraulic fracturing at the CY2 well indicates that the Carboniferous has good shale gas exploration potential. The QDD1 well shows an obvious gas logging anomaly in the Keluke Formation. Hence, it is necessary to systematically investigate pore structures and reservoir formation mechanism of the Keluke fine-grained reservoir with core samples from shallow drillings (ZK5-2, ZK1-1, ZK2-1, ZK3-2), the CY2 well, and the

QDD 1 well, which can deepen our understanding of shale-gas enrichment potential in this area.

## GEOLOGICAL SETTING

The Qaidam Basin with an area of approximately 120,000  $\text{km}^2$  is regarded as the largest intermontane basin in the Tibetan Plateau. Structurally, it is bounded by the South Qilian thrust belt at the northeast, the eastern Kunlun Shan–Qiman Tagh system at the southwest, and the left-lateral Altyn Tagh fault at the northwest. It is 3,000 m above mean sea level but is 1,000–2000 m lower than the surrounding mountains (Yin et al., 2002; Yin et al., 2008; Fang et al., 2007) (Figure 1A).

It is one of the important petroliferous sedimentary basins in northwest China, with an annual oil and gas yield of seven million tons oil equivalent since 2011 (Fu et al., 2015). The Delingha Depression in the east of the Qaidam Basin can be divided into five structural units by second-order faults and local structural traps, i.e., Oulongbruk Uplift, Onan Sag, Delingha Sag, Emnik Uplift, and Hobson Sag, which are NW-NWW extending alternately with a typical pattern of “three depressions

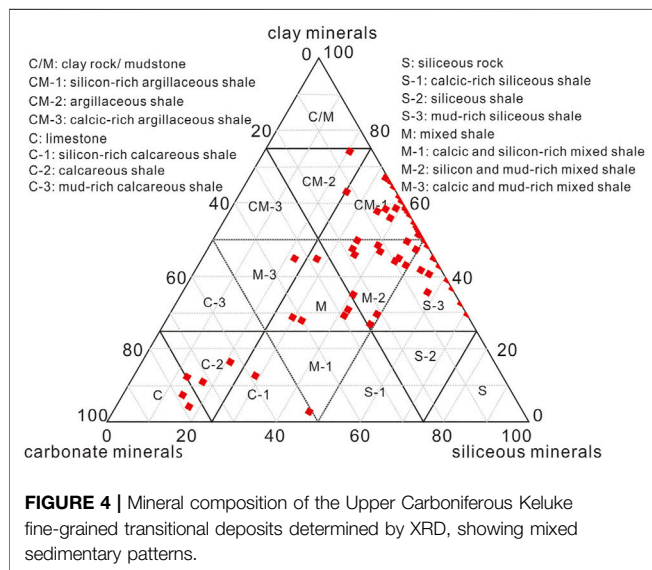
**TABLE 1 |** XRD analysis-based mineral compositions of fine-grained transitional deposits of the Upper Carboniferous Keluke Formation.

No	Depth/ m	Minerals and contents %								Lithology
		Quartz	Feldspar	Plagioclase	Calcite	Dolomite	Siderite	Pyrite	Clay minerals	
zk5-2-1	255	11.8	0.4	—	63	7.5	4.7	1	11.6	Argillaceous bioclastic limestone
zk1-1-1	309	33.6	2.6	1.7	2.2	—	2.3	7.1	50.5	Silty mudstone
zk2-1-1	731	31.6	1.6	1.9	—	—	4.6	2.9	57.4	Silty mudstone
zk1-1-2	221	17	1.4	1.8	4.8	—	6	6.5	62.5	Silt-bearing mudstone
CY2-1	658.58	37	1.9	2.2	—	—	—	2.2	56.7	Silty mudstone
CY2-2	1,021.7	39.6	1.5	3	—	—	5.3	2.8	47.8	Silty mudstone
CY2-3	844.75	44.4	0.8	2.3	3.1	—	4.6	2.3	42.5	Fine-grained lithic sandstone
CY2-4	980.9	42.5	1.2	3.1	—	—	1.6	3.6	48	Silty mudstone
CY2-5	910.57	16.3	—	0.8	64.5	4.7	—	3.1	10.6	Bioclastic limestone
CY2-6	996.5	25.3	0.8	3.5	2.4	14.5	31	3.7	18.8	Argillaceous-bearing siltstone
QDD1-8	1,507.94	43.2	5.7	3.5	1.8	5.2	0.6	2.2	37.8	Argillaceous siltstone
QDD1-9	1,313.8	22.5	2.9	4.2	1.9	8.9	1.3	1.5	56.8	Silty mudstone
QDD1-19	2,325	18.9	8.1	4.2	22.1	6.9	0.9	0	38.9	Calcareous-bearing argillaceous sandstone
QDD1-08	1,507.2	33.1	1.2	3.5	3.2	1.4	1.7	3.1	52.8	Silty mudstone
QDD1-15	1710.5	35.7	8.3	1.2	22.2	3.2	2.1	2.2	25.1	Calcareous-bearing argillaceous sandstone
QDD1-16	1,313.1	43.9	1.2	0.5	1.3	2.9	1.6	1.5	47.1	Silty mudstone
CY2-8	900.81	38.3	0.3	2.5	0.2	—	3.3	1.3	54.1	Sandy mudstone
CY2-9	902.91	31.2	—	1.7	0.8	—	0.3	1.5	64.5	Sandy mudstone
CY2-10	905.31	39.2	0.5	0.8	—	—	2.5	0.9	56.1	Sandy mudstone
CY2-11	907.37	45.5	0.2	3.4	—	—	—	2.5	48.4	Sandy mudstone
CY2-12	908.82	46.3	—	—	49.6	1.4	—	—	2.8	Sandy limestone
CY2-14	915.37	17.9	—	—	37.3	16.9	9.1	4.6	14.2	Dolomitic limestone
CY2-15	917	33.5	0.8	0.7	—	—	0.5	—	64.6	Sandy mudstone
CY2-16	918	40.3	0.7	2.2	—	—	0.6	1.3	54.9	Sandy mudstone
CY2-17	912.5	44	0.3	3.8	0.7	—	3.8	0.1	47.2	Argillaceous sandstone
CY2-20	927.65	47.1	0.3	1	13.7	10	—	2.1	25.9	Calcareous-bearing argillaceous sandstone
CY2-21	928.5	46.1	0.3	1.5	15.3	5	2.7	1.2	27.8	Calcareous-bearing argillaceous sandstone
CY2-22	931.85	13.8	—	—	61.5	16	—	1.4	7.3	Dolomitic limestone
CY2-23	934.6	42	0.7	4	—	—	4.7	1.9	46.6	Argillaceous sandstone
CY2-26	940.8	67.8	—	—	—	—	3.6	—	28.6	Argillaceous sandstone
CY2-27	943.5	60.5	—	0.8	—	—	—	—	38.7	Argillaceous sandstone
CY2-28	944.3	46.5	0.6	0.8	—	—	3.7	—	48.4	Argillaceous sandstone
CY2-29	945.8	35.4	0.5	1.8	—	10.5	2.4	6.4	43	Dolomite-bearing sandy mudstone
CY2-30	947.8	48.6	0.5	1.7	—	—	2.9	0.7	45.6	Argillaceous sandstone
CY2-31	950.2	50.3	0.6	1.7	1.8	3	0.2	3.1	39.3	Argillaceous sandstone
CY2-32	951.5	46.8	0.8	1.9	—	—	1.8	—	48.6	Argillaceous sandstone
CY2-33	953	45.4	0.6	2.9	—	—	1	—	50	Sandy mudstone
CY2-34	956	55.7	—	2.4	2.5	3.8	—	1.4	34.2	Argillaceous sandstone
CY2-35	956.8	52.6	0.4	1.7	—	3.5	0.3	3.3	38.2	Argillaceous sandstone
CY2-36	958.5	30.9	0.2	1.1	9.4	9.2	10.2	12.5	26.6	Lime and argillaceous-bearing sandstone
CY2-37	960.5	31	0.2	1.3	8.7	7.9	5.5	2.3	42.9	Calcareous-bearing sandy mudstone
CY2-38	962	30.4	0.3	1.8	6.4	—	10.3	0.5	50.2	Sandy mudstone
CY2-39	963.8	31.8	—	1.3	9.3	5.7	5.2	0.2	46.3	Calcareous-bearing sandy mudstone
CY2-40	965.6	25.2	0.5	1.2	9.2	17	4.8	0.6	41.5	Dolomite-bearing sandy mudstone
CY2-41	967.5	31.9	0.3	1.8	6.3	10.5	7.3	0.7	41.2	Dolomite-bearing sandy mudstone
CY2-44	970.1	29.7	—	—	26.3	11	4.7	2.4	25.8	Argillaceous-bearing sandy limestone
CY2-45	975.4	38.3	0.6	1.3	—	—	0.5	0.1	59.3	Sandy mudstone
CY2-46	975.5	45.3	0.4	0.9	8.5	—	1.1	—	43.8	Argillaceous sandstone
CY2-47	978	48.1	0.3	0.6	0.3	—	1.5	9.6	39.5	Argillaceous sandstone
CY2-49	985.9	36.6	0.6	1	—	4.9	4.1	0.2	52.6	Sandy mudstone
CY2-50	986.9	42.8	0.7	1.2	—	—	2.2	4.7	48.5	Sandy mudstone
CY2-51	990.3	36.5	0.4	4.1	—	10.8	0.3	6.3	41.5	Dolomite-bearing argillaceous sandstone
CY2-52	992.3	16.8	—	—	57.7	19.9	—	1.5	4.2	Dolomitic limestone
CY2-53	994	44	—	1.1	4.6	5	0	2.9	42.2	Argillaceous sandstone
CY2-55	999	40.2	—	1.3	—	—	1.2	4.5	52.8	Sandy mudstone
CY2-56	1,002.5	44.7	0.4	0.7	—	—	2.4	—	51.8	Sandy mudstone
CY2-57	1,004.5	56.2	—	0.5	—	—	1	—	42.2	Argillaceous sandstone
CY2-58	1,006.5	59.8	0.4	—	—	—	5.1	—	34.7	Argillaceous sandstone
CY2-59	1,007	67.3	—	—	—	—	0.1	—	32.6	Argillaceous sandstone

(Continued on following page)

**TABLE 1 |** (Continued) XRD analysis-based mineral compositions of fine-grained transitional deposits of the Upper Carboniferous Keluke Formation.

No	Depth/ m	Minerals and contents %								Lithology
		Quartz	Feldspar	Plagioclase	Calcite	Dolomite	Siderite	Pyrite	Clay minerals	
CY2-61	1,016.6	25.6	0.2	3.1	7.7	28.8	6.4	3.2	25	Argillaceous-bearing sandy dolomite
CY2-63	1,024.2	40.3	0.3	1.4			2.7	0.4	54.9	Sandy mudstone
CY2-64	1,029	28.1			41.9	15.9		1.5	12.5	Dolomite-bearing sandy limestone
CY2-67	1,034.7	32.7	0.4	1.3			12	0.7	53	Sandy mudstone
CY2-68	1,042.3	46.9	0.3	1.7			3.8	0.7	46.5	Argillaceous sandstone

**FIGURE 4 |** Mineral composition of the Upper Carboniferous Keluke fine-grained transitional deposits determined by XRD, showing mixed sedimentary patterns.

alternating with two uplifts” (Figures 1B,C). The Proterozoic, Paleozoic, and Mesozoic successions are widely developed in the Delingha Depression, where the deeply buried and widely distributed Carboniferous is overlain by the Jurassic with no Permian or Triassic. The fault system is dominated by reverse faults. The Carboniferous system is commonly deeply buried and widely distributed in the depression. Mature to high mature mudstone prevails in the Upper Carboniferous Keluke and Zhabusagaxiu transitional coal measures with high TOC and type II<sub>2</sub> and type III kerogen (Cao et al., 2016; Liu et al., 2016).

The Keluke-1 Member ( $C_2k^1$ ) can be lithologically divided into two sections, i.e., the lower is carbonaceous shale interbedded with coal seams and the upper is stripped micrite, which was primarily deposited at shore, tidal flat, peat flat, and mixed tidal flat setting. The Keluke-2 Member ( $C_2k^2$ ) is composed of micrite with grey mudstone interbedded with thin coal seams (thickness <3 m). It was mainly derived from shore, tidal flat, and mixed tidal flat environments. The Keluke-3 Member ( $C_2k^3$ ) is mainly sand-conglomerate and sandstone alternating with dark mudstone, carbonaceous shale, and coal seams, which were deposited at shore, barrier island, and tidal flat environment. The Keluke-4 Member ( $C_2k^4$ ) is dominated by dark carbonaceous shales laminated with thin limestone and coal seams from shore and tidal flat environment (Figure 2).

## SAMPLES AND METHODS

There were 64 core samples from shallow drillings (ZK5-2, ZK1-1, ZK2-1, ZK3-2), the CY2 well, and the QDD 1 well taken to conduct the porosity and permeability test and the X-ray diffraction (XRD) analysis. Then, some samples were selected to carry out Quantitative Mineral Evaluation via Scanning Electron Microscopy (QEMSCAN), Field Emission Scanning Electron Microscopy (FESEM), and combined N<sub>2</sub> adsorption and high-pressure mercury injection (MICP).

A PoroPDP-200 full-automatic instrument was used to determine porosity and permeability under various confining pressures. There were 3 cm plugs drilled from cores. Porosimeter can be used to calculate porosity (from 0.01% to 40%) based on Boyle’s Law and the principle of helium gas expansion, under operation pressure of 0 MPa–0.7 MPa. The permeability measurement based on the pulse decay technique can measure permeability ranging from 0.00001 to 10 mD, while confining pressure increases from 7 to 32 MPa under a constant pore pressure of 7 MPa.

An XRD experiment was performed using a ZJ207 Bruker D8 advance X-ray diffractometer following the Oil and Gas Industry Standards (SY/T5463-2010). Shale samples were crushed into smaller than 300 mesh and were mixed with ethanol in a mortar and pestle, then smear-mounted on glass slides for XRD analysis. The X-ray diffractometer with Cu X-ray tube was operated at 40 kV and 30 mA and was scanned from 2 to 70° at a step of 0.02°, and data was semi-quantified using Jade 6.0 software.

Two shale samples were mineralogically imaged by QEMSCAN at standard (5 μm) and high (1 μm) resolution. Large standard resolution images can better express rock properties as a whole, whereas high-resolution images can give more details about rock fabric, mineral associations, and lithology. The higher resolution images also underestimate porosity as the area imaged represents a small unit of the whole sample. Hence, the standard resolution measurements provide the reference mineralogical, density, and porosity data; the data for the detailed measurements are provided for reference only.

Thin sections were examined under both transmitted light and reflected light using a Zeiss microscope instrument. FESEM was used to observe micro- and nano-sized pores. All shale samples were crushed into flakes measuring approximately 10 × 10 × 3 mm by using a stone-cutting machine, which were observed directly without being polished. Sample surfaces were coated with 10 nm thick gold to enhance electrical conductivity before the

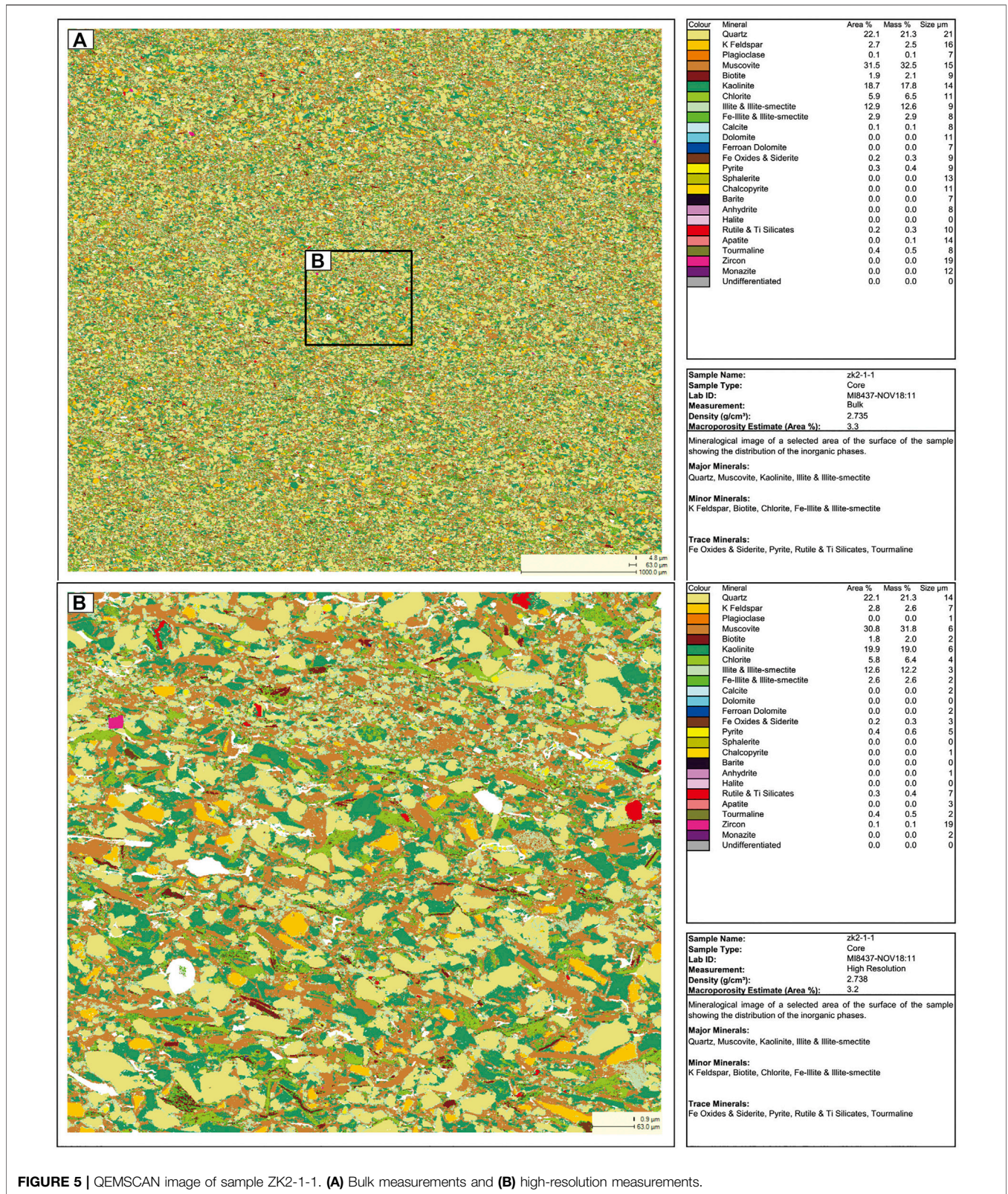


FIGURE 5 | QEMSCAN image of sample ZK2-1-1. (A) Bulk measurements and (B) high-resolution measurements.

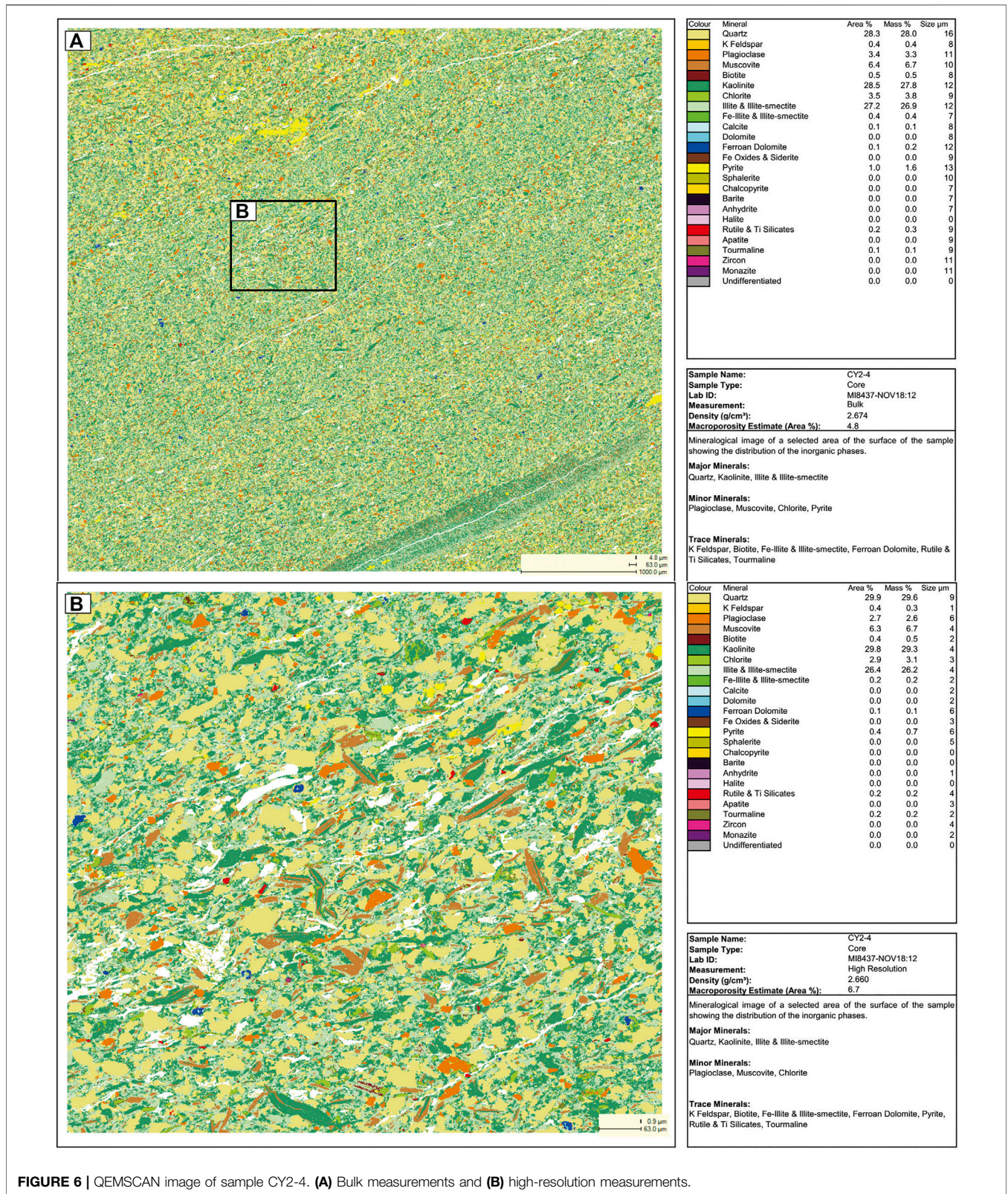
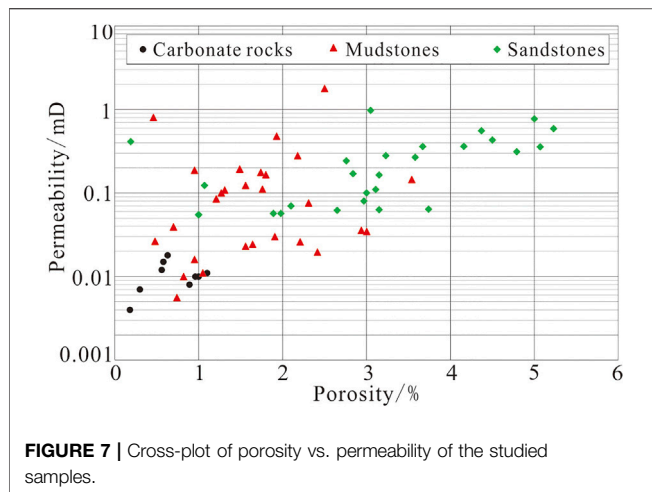


FIGURE 6 | QEMSCAN image of sample CY2-4. (A) Bulk measurements and (B) high-resolution measurements.



observation. The experiments were conducted using an FEI Quanta200F scanning electron microscope, with a maximum resolution of 1.2 nm and a maximum magnification of 0.2 million times. All SEM observations were performed following the Chinese oil and gas industry standard SY/T 5162–2014.

Low-pressure gas ( $N_2$ ) adsorption and MICP were carried out to determine pore size distribution (PSD) following NB/T 14008–2015. PSDs derived from mercury porosimetry (pore radius of 6–10,000 nm) and low-pressure gas adsorption (pore radius of 1–10 nm) were normalized and connected at 6 nm based on porosity parameters, expressing PSDs in a range of 1–10,000 nm. Gas-water capillary pressure can be converted from gas-mercury capillary pressure with surface tensions of water and mercury, obtaining a full-pore capillary pressure curve. Consequently, breakthrough pressure and other parameters can be interpreted.

## RESULTS

### Mineralogy and Petrography

Core observation and thin section identification show that the Upper Carboniferous Keluke Formation in the Eastern Qaidam Basin varies greatly in lithology, forming typical mixed rock and mixed sequences (Figure 3), e.g., siltstone, fine sandstone, calcareous siltstone, argillaceous siltstone, silty mudstone, mudstone, carbonaceous mudstone, coal, bioclastic limestone, marlstone, shell-bearing silty mudstone, lime-bearing argillaceous siltstone, dolomite-bearing silty mudstone, silty-bearing dolomite, and dolomite-bearing limestone.

Measured typical XRD patterns and mineral compositions are shown in Table 1. Generally, the Keluke fine-grained samples vary greatly in mineral compositions, where carbonate minerals, e.g., calcite and dolomite, widely developed with subordinate aragonite, siderite, and magnesite. Various rock types are identified from samples, e.g., mudstone, lime mudstone, argillaceous siltstone, lime siltstone, siltstone, fine sandstone (dominated by lithic arenite and lithic wacke), and marlstone. The Upper Carboniferous Keluke fine-grained transitional shales

behave as typically mixed rocks and mixed sequences (Figure 4), which is consistent with thin section identification.

Two shale samples were mineralogically imaged by QEMSCAN at standard (5  $\mu\text{m}$ ) and high (1  $\mu\text{m}$ ) resolution. Sample ZK2-1-1 is generally dominated by coarse- and silt-grade quartzes and K-feldspar grains with muscovite and kaolinite (Figure 5). Grain-like kaolinite is a good indicator of grain replacement (e.g., plagioclase alteration and replacement). Flake-like muscovite is mixed with illite as a matrix surrounding silt grains. Biotite flakes are popular, whereas some are partially altered to, or completely replaced with, chlorite. Both muscovite and biotite flakes are parallel to weak bedding. Moderate amounts of macropores are recorded (3.3 area %), occurring as voids and fractures parallel to bedding. Pores are generally bedding-parallel connected but are poorly connected in vertical.

For CY2-4 in Figure 6, this finely laminated silty mudstone is characterized by subangular to subrounded quartz and plagioclase grains surrounded by illite mixed with kaolinite. Different from most samples analyzed, K feldspar is not popular in this sample. Large muscovite grains occur throughout, typically parallel to laminations. Considerable chlorite particles but no biotite indicate that the latter may have been altered and/or replaced. Most illite presents as an intergranular matrix, whereas some occur as grain-like particles. Ferroan dolomite grains are prevailing and pyrite framboids are also widely developed. Macro pores (4.8 area %) are associated with plate-like pores representing bedding-parallel fractures.

### Porosity and Permeability

Petrophysical property measurement on 64 Keluke fine-grained rocks shows that porosity is in the range of 0.19–5.23% (average 2.13%), and permeability is in the range of 0.01–1  $\times 10^{-3} \mu\text{m}^2$  (average 0.19  $\times 10^{-3} \mu\text{m}^2$ ), which are lower than typical marine shales and are roughly equivalent with other transitional shales (Luo et al., 2018). A positive correlation can be observed between porosity and permeability. Sandstones have the highest porosity, in the range of 0.19–5.23% (average 3.16%), while mudstones have lower porosity (0.46–3.54%, average 1.65%). Carbonate rocks have the lowest values of 0.19–1.1%, averaging 0.65% (Figure 7). Permeability follows a similar variation, while mudstone has a great variation in permeability. Porosity and permeability of mudstone samples are poorly correlated with each other, which may be caused by mineral composition and diagenesis of different sedimentary facies.

## PORE STRUCTURE CHARACTERIZATION

### Pore Types

Pores in shale can be classified as 1) organic-matter-hosted pores, 2) interparticle pores (pores between grains and crystals), 3) intraparticle pores (pores within grains, crystals, and clay aggregates), and microfractures (Loucks et al., 2012; Ko et al., 2016). FE-SEM observation identifies various pore types and pore sizes in the studied samples, e.g., residual interparticle and intercrystalline pores, interparticle and intraparticle dissolution pores, etc.

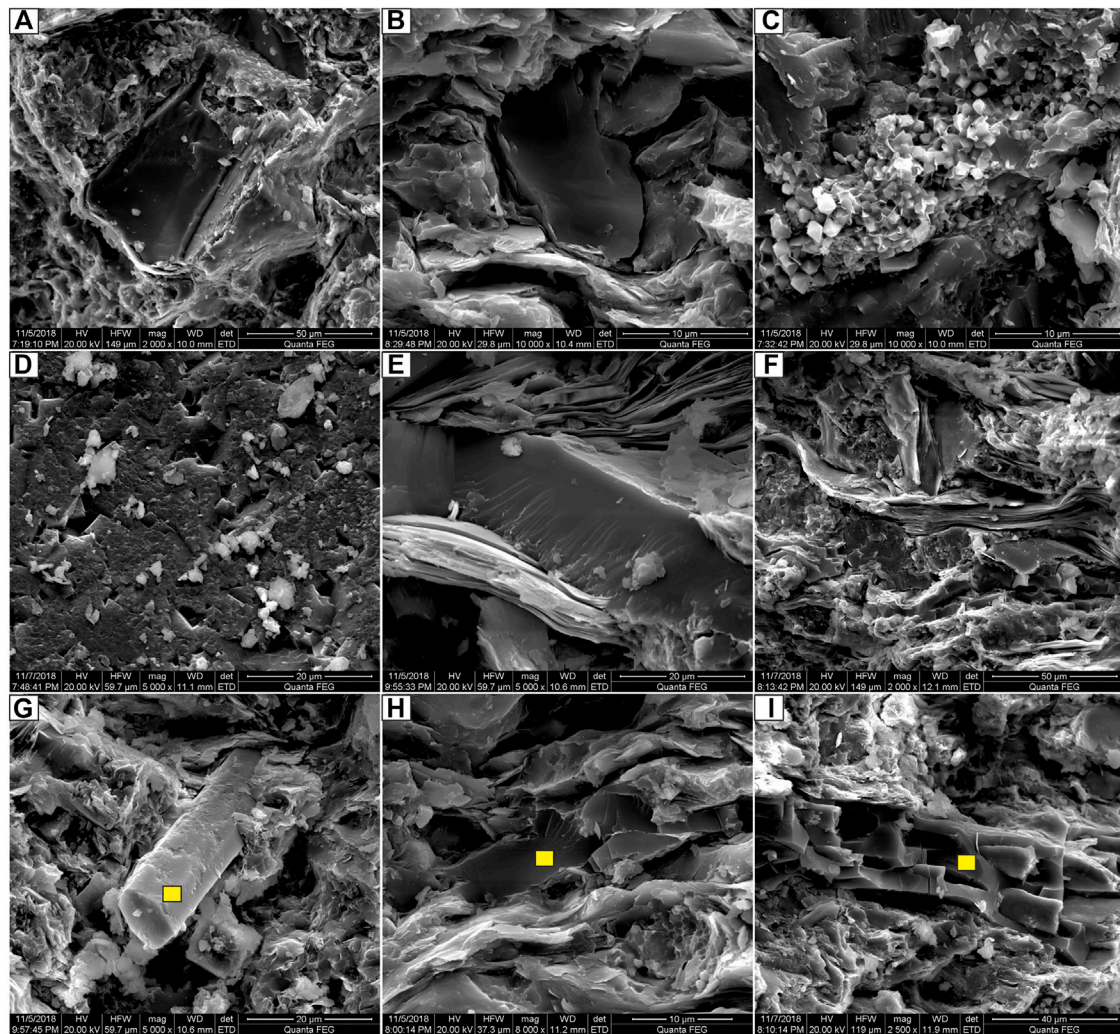


**FIGURE 8** | FESEM images, energy spectrum, and thin-section photomicrographs of the Upper Carboniferous Keluke transitional shales. **(A)** Siliceous grains and associated pores. **(B)** Micro-scale organic matter (coal cuttings), interparticle pores. **(C)** Nano-scale pyrite aggregate. **(D)** Calcite and associated intergranular pores. **(E)** Siliceous grains, slit-like minerals, and associated pores. **(F)** Slit-like minerals (chlorite and mica), coal seam intermixed with grained minerals (carbonate minerals), interparticle pores. **(G)** Columnar minerals (detrital aluminite minerals) and alteration products. **(H)** Micro-scale organic matter (coal cuttings), short stripe along bedding, interparticle pores, no pore in organic matter. **(I)** Coal cuttings (fusinite) intermixed with mudstone (clay minerals). **(J–L)** energy spectrums of minerals marked by yellow boxes in **(G–I)**, respectively. **(M)** Pyrites and associated pores, fractures along bedding. **(N)** Nano-scale dissolution pores in calcite. **(O)** Broken organic matter (coal and vitrinite) and conchoidal fracture. **(P)** Organic matter and its internal structure show nano-scale spherical structure (asphaltite?). **(Q,R)** Fractures and laminas.

Interparticle and intercrystalline pores are the most popular ones, e.g., pores between siliceous particles and carbonate minerals, pores between organic matter and surrounding minerals (or shrinkage joint of organic matter), and pores supported by some special minerals. Interparticle pores are primarily associated with pyrites and clay minerals. The dissolution pores observed are contributed by pyrite falling and calcite dissolution (**Figure 8**). A large amount of organic matter (mainly vitrinite, with fusinite of secondary importance) can be identified from samples, while bitumen with nano-spherical structure can be found occasionally. However, organic-matter-hosted pores are not found, while only pores among organic matter frameworks can be observed from fusinite. Well-preserved original cell architecture can be

observed, presenting as network or sieve-like. Different types of micro-fractures are also widely developed, e.g., bedding fractures, structural fractures, and dissolution fractures, where tectonic fractures connect different fractures in local positions (**Figure 8**).

## Pore Size Distributions

Although SEM can directly image individual pores or provide information on their mode, it cannot demonstrate pore size distributions. Pore size characterization is commonly performed with indirect petrophysical methods such as MICP measurements, nitrogen/CO<sub>2</sub> adsorption, and nuclear magnetic resonance (NMR) spectroscopy (Loucks et al., 2012; Yang et al., 2017; Song et al., 2019). Pores with size less than 2 nm are

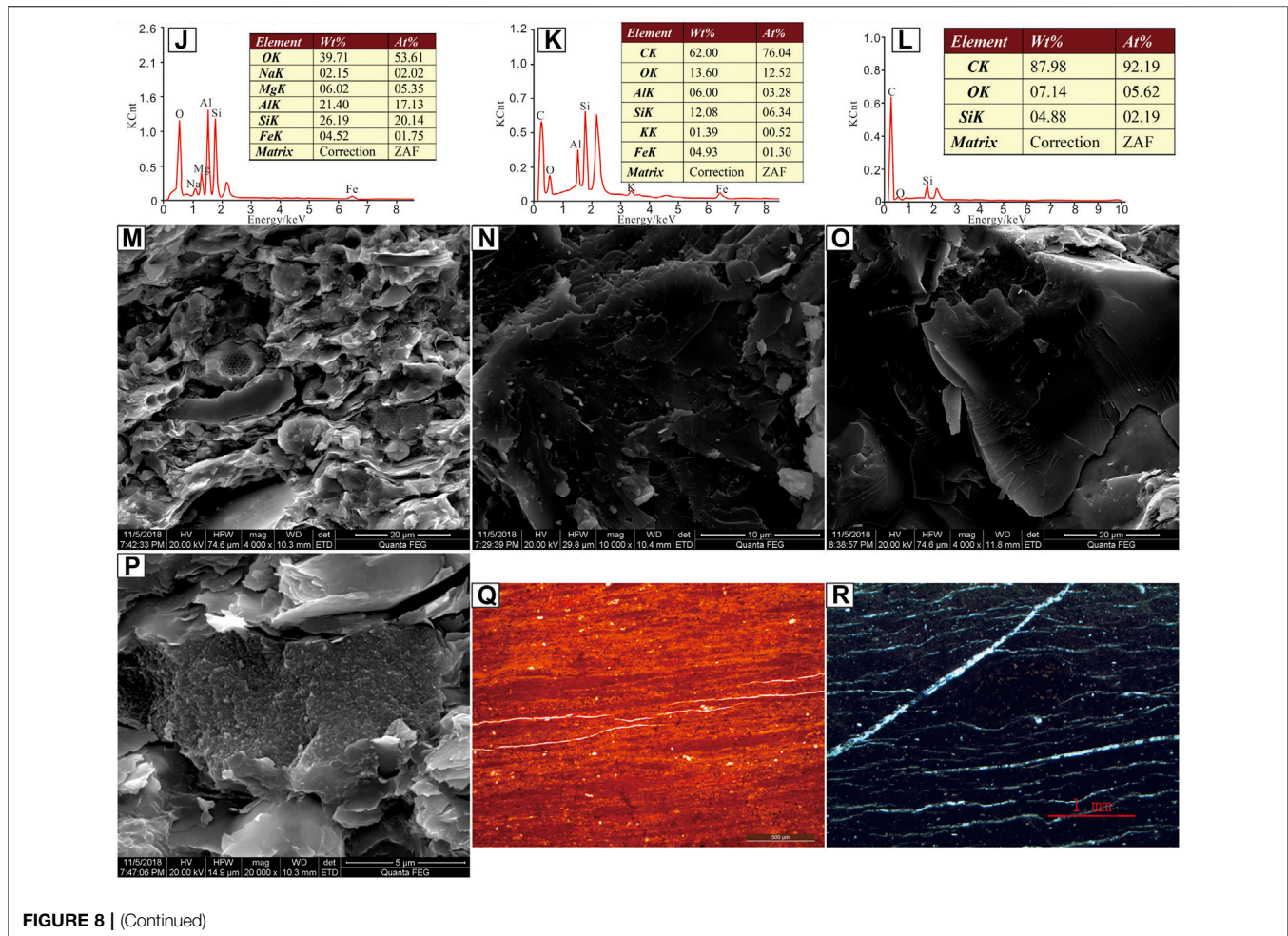


FIGURE 8 | (Continued)

assumed to be undeveloped in Keluke Shales since organic pores are not well developed. Hence, the CO<sub>2</sub> adsorption experiment was not carried out to obtain pore size < 2 nm, while MICP and nitrogen adsorption were performed on four samples with different lithologies.

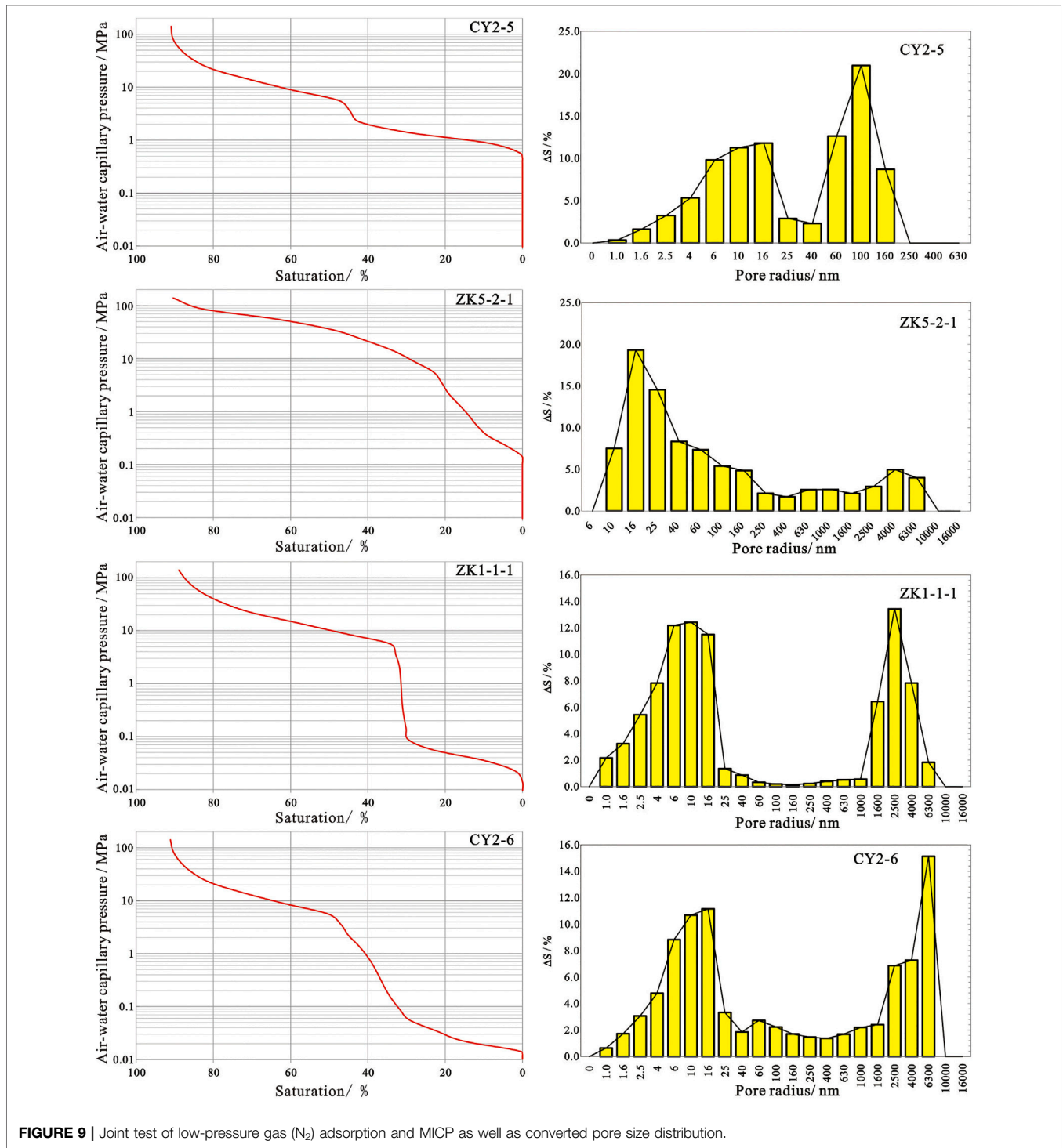
The PSD of Keluke fine-grained rocks follows a bimodal pattern, which is not obvious in some samples. The PSD of argillaceous bioclastic limestone (ZK5-2-1) is a weak bimodal pattern, while the peak of mesoporous and macropore is concentrated at 16–25 nm and at about 4,000–6,000 nm, respectively. The PSD of silty mudstone (ZK1-1-1) exhibits an obvious bimodal pattern, with peak values at 6–16 and 2,500 nm, respectively. For bioclastic limestone (CY2-5), the peak value of mesopores and macropores is centered at 6–16 nm and at about 100 nm, respectively, which is smaller compared with other lithologies. For argillaceous siltstone (CY2-6), the peak of mesopores is at 6–16 nm, while that of macropores is at about 6,000 nm (Figure 9). Breakthrough pressure and median pressure refer to capillary pressures at cumulative saturation of 10% and 50% under gas-water conditions, respectively. Argillaceous bioclastic limestone and bioclastic limestone have large breakthrough pressure and small breakthrough radius,

indicating a small proportion of macropores (Table 2). Hence, bioclastic limestone has worse reservoir quality compared with other lithologies. Sandstone and mudstone show an obvious bimodal pattern with a similar proportion of macropores and mesopores, indicating that sandstone and mudstone have stronger heterogeneity than bioclastic limestone.

## DISCUSSION

### Factors Affecting Organic Pore Development

Previous studies suggested that organic pores were not developed in all organic matter, which was controlled by both organic macerals and thermal maturity (Curtis, 2002; Gao et al., 2019; Song et al., 2019; Cavelan et al., 2019; Katz and Arango, 2018). The vitrinite reflectance (R<sub>v</sub>) of Keluke Shales is higher than 1.3% in the study area, e.g., >1.6% at the CY2 well, and >2.0% at the QDD 1 well, which is higher than the threshold value of organic pore growth. Therefore, thermal maturity is not the controller of organic pore development in Keluke Shales in the study area.

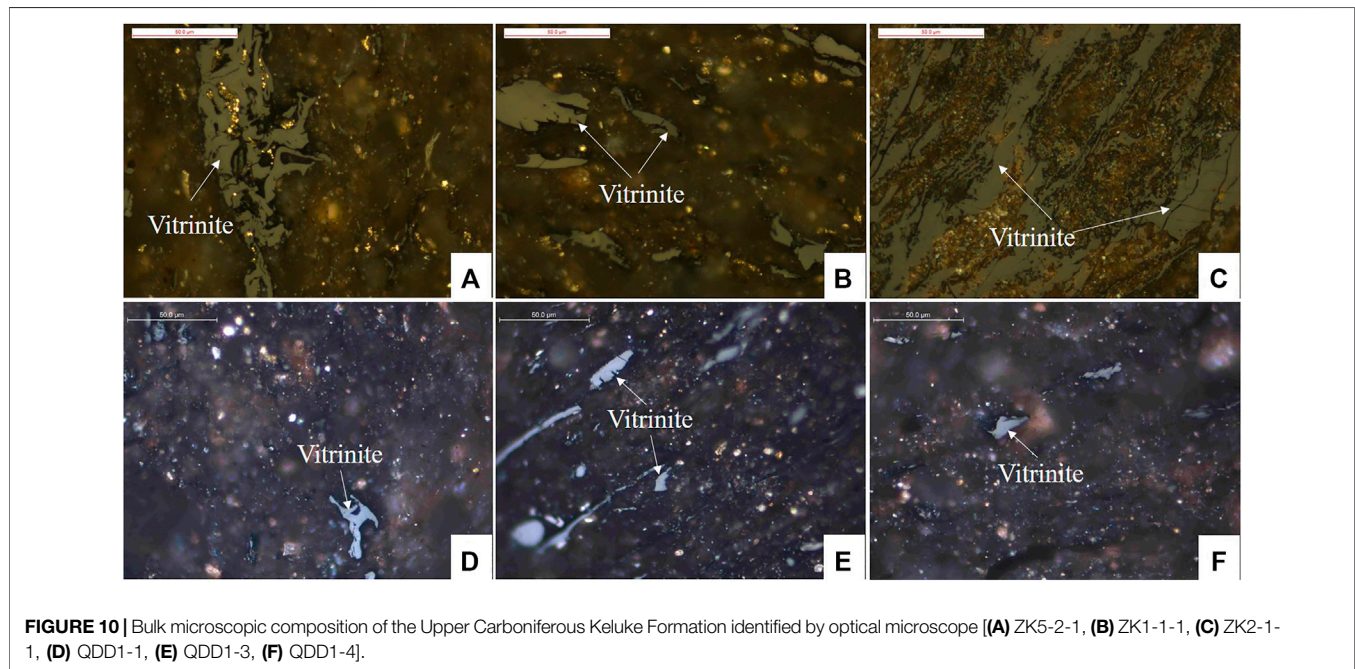


The organic pore development is essentially related to hydrocarbon generation potential of different organic macerals, e.g., sapropelinite and exinite have the largest hydrocarbon generation potential, vitrinite is primarily gas-prone, inertinite almost has no hydrocarbon generation capacity, and solid bitumen can be cracked into light oil and natural gas (Behar et al., 2008; Ko et al., 2016). Organic matter in

Keluke Shales is dominated by vitrinite with minor inertinite (Figure 10), where vitrinite is mainly composed of vitrodetrinite or striped collinite, with a small group of desmocollinite and corpocollinite. The inertinites are mainly inertodetrinite, coexisting with vitrinite. This agrees well with coal cuttings identified under the scanning electron microscope (Figure 8), where no organic pores are developed. It is different from

**TABLE 2** | Reprehensive parameters of jointed low-pressure gas (N<sub>2</sub>) adsorption and MICP measurements.

Sample	Lithology	Sedimentary facies	Parameters			
			Breakthrough pressure/MPa	Breakthrough radius/nm	Median pressure/MPa	Median radius/nm
CY2-5	Bioclastic limestone	Restricted platform	0.91	154.20	6.28	22.31
zk5-2-1	Argillaceous bioclastic limestone	Mixed flat	0.42	329.99	36.44	3.84
zk1-1-1	Silty mudstone	Lagoon	0.04	3,941.68	10.58	13.23
CY2-6	Argillaceous siltstone	Sand flat	0.02	7,202.82	5.46	25.64



representative marine gas shales worldwide, where many organic pores are developed (mostly in solid bitumen) (Inan et al., 2018; Katz and Arango, 2018; Guo et al., 2019). However, XRD identification and SEM observation show no solid bitumen at high to over-high maturity stage in the study area. This may be attributed to type-III kerogen in the Keluke Shales with few oil-prone macerals. In other words, organic pore development varies as a function of kerogen types. Generally, organic pores are the worst developed in transitional shale compared with marine and continental shales.

### Favorable Lithofacies in the Marine–Continental Transitional Shales

The analysis above shows that the Keluke Formation is a set of mixed sequences, and thereby, determining favorable lithofacies is essential to seek sweet spots. The Keluke sequences were deposited in tidal flat, lagoon, restricted platform, and barrier island. Low-energy clastic coast (including tidal flat and lagoon), mixed restricted platform, and mixed shelf were developed in the lower section of the Keluke Formation, and mixed sandy clastic

coast with barrier bar, mixed restricted platform, as well as a mixed shelf were developed in the middle-upper section (Chen et al., 2016b).

Sedimentary facies play an important role in controlling pore growth because it not only governs deposition pattern, but also controls mineral compositions and contents, as well as determines diagenesis to a large extent (HallCraig, 2019; Gogoi and Rima, 2020). The cross plot of porosity and permeability shows that reservoir quality is the best in sandstone, followed by mudstone, and is the worst in carbonate rocks. Porosity is positively correlated with quartz content and is negatively correlated with clay mineral content. A poor correlation can be observed between it and carbonate mineral content. This can be explained by following reasons. Intensive hydrodynamics, low organic matter content, and high carbonate and quartz content can result in high porosity in deposits from barrier bar and tidal delta. Deposits from low-energy lagoon with no organic pore has low porosity. Rocks from sand flat and tidal channel with intensive hydrodynamics generally have coarse particles, resulting in high porosity. Mixed flat and mud flat have weaker hydrodynamic conditions, resulting in finer deposits

with the lowest porosity. The thin section identification and XRD analysis show that weak hydrodynamics in the restricted platform can deposit fine-grained rocks, e.g., argillaceous limestone, silty limestone, micrite, bioclastic-bearing micrite, and bioclastic micritic, with poor physical property when no dissolution and dolomitization occur to them. Intensive carbonate cementation is common in shale from tidal flat intersected with restricted platform, which is not conducive to primary pore preservation and can decrease porosity significantly.

## CONCLUSION

In this study, we comprehensively investigated mineralogy and pore structure of the Upper Carboniferous Keluke marine-continental transitional shales. Controlling factors of pore development in shale reservoir were discussed based on detailed analysis of reservoir properties, and organic pore development in transitional shales and typical marine shales were compared. The conclusions obtained from this study are as follows:

- 1) The Upper Carboniferous marine-continental transitional strata consists of complex interbedded sandstone, shale, coal, and limestone. The complex mineral compositions result in typically mixed rocks and mixed sequences. The porosity of Keluke fine-grained rocks is in a range of 0.5–5% and permeability is in a range of  $0.01\text{--}1\times 10^{-3}\ \mu\text{m}^2$ , which is the highest in sand laminae.
- 2) Considerable interparticle and intercrystalline pores with minor dissolution pores and micro-fractures are developed in the Keluke transitional shales. Pores associated with organic matter frameworks can be found. Particularly, vitrinite and inertinite are the dominant organic macerals in Keluke Shales, which limits secondary organic pore development.
- 3) The PSDs of fine-grained rocks in the Keluke Formation follow a bimodal pattern, while dominated pore sizes vary greatly with lithologies. The proportion of micro-scale pores

and macro-scale nanopores increases in an order: bioclastic limestone, argillaceous bioclastic limestone, silty mudstone, argillaceous siltstone. The differences in pore structure are attributed to the sedimentary facies and associated mineralogy and diagenesis.

## DATA AVAILABILITY STATEMENT

The original contributions presented in the study are included in the article/supplementary material, further inquiries can be directed to the corresponding author.

## AUTHOR CONTRIBUTIONS

YG: Conducted experiments, Data analysis, Visualization, Writing—original draft, Project administration. XF: Conceptualization, Methodology, Supervision, Data analysis, Visualization, Writing—original draft. HW: Resources, Project administration. NW: Resources, Project administration.

## FUNDING

This study is supported by the China National Natural Science Foundation (NOs. 41972160 and 42172176), and the open fund of Hubei Key Laboratory of Marine Geological Resources, China University of Geosciences (MGR202007).

## ACKNOWLEDGMENTS

The reviewers are gratefully acknowledged for constructive comments that substantially improved the quality of this manuscript. Also, we appreciate Dr. Dongdong Liu, the Guest Associate Editor, for suggestions to revise this manuscript.

## REFERENCES

- Abdel-Fattah, Z. A., Kora, M. A., and Raafat, S. A. (2018). Depositional Environments and Sequence Stratigraphy of a Mixed Siliciclastic-Carbonate Ramp: An Example from the Cenomanian to Turonian Galala Formation in the Northern Eastern Desert, Egypt. *J. Afr. Earth Sci.* 147, 352–373. doi:10.1016/j.jafrearsci.2018.06.029
- Behar, F., Lorant, F., and Lewan, M. (2008). Role of NSO Compounds during Primary Cracking of a Type II Kerogen and a Type III lignite. *Org. Geochem.* 39, 1–22. doi:10.1016/j.orggeochem.2007.10.007
- Boggs, S., Jr (2012). *Principles of Sedimentology and Stratigraphy [M]*. 5th ed. Boston: Pearson India.
- Cao, J., Liu, C. L., and Ma, Y. S. (2016). Geochemical Characteristics and Genesis of Shale Gas for Carboniferous marine-continental Transitional Facies Coal Measure Strata in Eastern Qaidam Basin. *Earth Sci. Front.* 23 (5), 158–166. (in Chinese, English abstract). doi:10.13745/j.esf.2016.05.017
- Cavelan, A., Boussafir, M., Milbeau, C. L., Rozenbaum, O., and Laggoun-Défarge, F. (2019). Effect of Organic Matter Composition on Source Rock Porosity during Confined Anhydrous thermal Maturation: Example of Kimmeridge-clay Mudstones. *Int. J. Coal Geology.* 212, 103236. doi:10.1016/j.coal.2019.103236
- Chalmers, G. R., Bustin, R. M., and Power, I. M. (2012). Characterization of Gas Shale Pore Systems by Porosimetry, Pycnometry, Surface Area, and Field Emission Scanning Electron Microscopy/Transmission Electron Microscopy Image Analyses: Examples from the Barnett, Woodford, Haynesville, Marcellus, and Doig Units. *Bulletin* 96 (6), 1099–1119. doi:10.1306/10171111052
- Chen, S. Y., Liu, J., and Ma, S. (2016a). Characteristics of Keluke Shales Reservoirs in Northeast Margin of Qaidam Basin. *Earth Sci. Front.* 23 (5), 56–65. (in Chinese, English abstract). doi:10.13745/j.esf.2016.05.006
- Chen, S. Y., Sun, J. P., and Bi, M. W. (2016b). Mixed Sedimentary Characteristics and Controlling Factors of Upper Paleozoic Group in Northern Qaidam Basin. *Geol. Bull. China* 35 (2/3), 282–292. (in Chinese, English abstract). doi:10.3969/j.issn.1671-2552.2016.02.010
- Curtis, J. B. (2002). Fractured Shale-Gas Systems. *AAPG Bull.* 86, 1921–1938. doi:10.1306/61eeddbe-173e-11d7-8645000102c1865d
- Dai, J., Zou, C., Dong, D., Ni, Y., Wu, W., Gong, D., et al. (2016). Geochemical Characteristics of marine and Terrestrial Shale Gas in China. *Mar. Pet. Geology.* 76, 444–463. doi:10.1016/j.marpetgeo.2016.04.027
- Dong, D. Z., Qiu, Z., Zhang, L. F., Li, S. X., Zhang, Q., Li, X. T., et al. (2021). Progress on Sedimentology of Transitional Facies Shales and New Discoveries of Shale Gas. *Acta Sedimentologica Sinica* 39 (1), 29–45. (in Chinese, English abstract). doi:10.14027/j.issn.1000-0550.2021.002
- EIA (2013). *Technically Recoverable Shale Oil and Shale Gas Resources: An Assessment of 137 Shale Formations in 41 Countries outside the United State*. Available from: <http://www.eia.gov/analysis/studies/worldshalegas/>.

- Fang, X., Zhang, W., Meng, Q., Gao, J., Wang, X., King, J., et al. (2007). High-resolution Magnetostratigraphy of the Neogene Huaitoutala Section in the Eastern Qaidam Basin on the NE Tibetan Plateau, Qinghai Province, China and its Implication on Tectonic Uplift of the NE Tibetan Plateau. *Earth Planet. Sci. Lett.* 258, 293–306. doi:10.1016/j.epsl.2007.03.042
- Fu, S., Ma, D., Guo, Z., and Cheng, F. (2015). Strike-slip Superimposed Qaidam Basin and its Control on Oil and Gas Accumulation, NW China. *Pet. Exploration Dev.* 42 (6), 778–789. doi:10.1016/s1876-3804(15)30074-4
- Galloway, W. E. (1998). Clastic Depositional Systems and Sequences: Applications to Reservoir Prediction, Delineation, and Characterization. *The Leading Edge* 17, 173–180. doi:10.1190/1.1437934
- Gao, F. L., Song, Y., and Liang, Z. K. (2019). Development Characteristics of Organic Pore in the continental Shale and its Genetic Mechanism: a Case Study of Shahezi Formation Shale in the Changling Fault Depression of Songliao Basin. *Acta Petrolei Sinica* 40 (9), 1030–1044. (in Chinese, English abstract). doi:10.7623/syxb201909002
- Gentzis, T. (2013). A Review of the thermal Maturity and Hydrocarbon Potential of the Mancos and Lewis Shales in Parts of New Mexico, USA. *Int. J. Coal Geology.* 113, 64–75. doi:10.1016/j.coal.2012.09.006
- Gogoi, T., and Chatterjee, R. (2020). Multimineral Modeling and Estimation of Brittleness Index of Shaly Sandstone in Upper Assam and Mizoram Areas, India. *SPE Reservoir Eval. Eng.* 23, 708–721. doi:10.2118/200498-pa
- Guo, X. S., Hu, D. F., and Liu, R. B. (2018). Geological Conditions and Exploration Potential of Permian marine-continent Transitional Facies Shale Gas in the Sichuan Basin. *Nat. Gas Industry* 38 (10), 17–24. (in Chinese, English abstract). doi:10.3787/j.issn.1000-0976.2018.10.002
- Guo, X., Qin, Z., Yang, R., Dong, T., He, S., Hao, F., et al. (2019). Comparison of Pore Systems of clay-rich and Silica-Rich Gas Shales in the Lower Silurian Longmaxi Formation from the Jiaoshiba Area in the Eastern Sichuan Basin, China. *Mar. Pet. Geology.* 101, 265–280. doi:10.1016/j.marpetgeo.2018.11.038
- HallCraig, C. D. (2019). “Compositional and Diagenetic Controls on Brittleness in Organic Siliceous Mudrocks,” in *Mudstone Diagenesis: Research Perspectives for Shale Hydrocarbon Reservoirs, Seals, and Source Rocks: AAPG Memoir 120*. Editors W. Camp, K. Milliken, K. Taylor, N. Fishman, P. Hackley, and J. Macquaker, 103–120. doi:10.1306/13672213m1213823
- Harratz, H. Z. (2013). *Introduction to Sedimentary Ore Deposits*. Tanta: Online Presentation. doi:10.13140/RG.2.1.1035.8640
- Inan, S., Al Badairy, H., Inan, T., and Al Zahrani, A. (2018). Formation and Occurrence of Organic Matter-Hosted Porosity in Shales. *Int. J. Coal Geology.* 199, 39–51. doi:10.1016/j.coal.2018.09.021
- Jarvie, D. M., Hill, R. J., Ruble, T. E., and Pollastro, R. M. (2007). Unconventional Shale-Gas Systems: the Mississippian Barnett Shale of north-central Texas as One Model for Thermogenic Shale-Gas Assessment. *Bulletin* 91 (4), 475–499. doi:10.1306/12190606068
- Jiang, S., and Tang, X. L. (2017). Enrichment Factors and Current Misunderstanding of Shale Oil and Gas: Case Study of Shales in U.S., Argentina and China. *J. China Univ. Geosciences* 42 (7), 1083–1091. (in Chinese, English abstract). doi:10.3799/dqkx.2017.087
- Katz, B. J., and Arango, I. (2018). Organic Porosity: A Geochemist’s View of the Current State of Understanding. *Org. Geochem.* 123, 1–16. doi:10.1016/j.orggeochem.2018.05.015
- Ko, L. T., Loucks, R. G., Zhang, T., Ruppel, S. C., and Shao, D. (2016). Pore and Pore Network Evolution of Upper Cretaceous Boquillas (Eagle Ford-equivalent) Mudrocks: Results from Gold Tube Pyrolysis Experiments. *Bulletin* 100, 1693–1722. doi:10.1306/04151615092
- Kuang, L. C., Dong, D. Z., and He, W. Y. (2020). Geological Characteristics and Development Potential of Transitional Shale Gas in the East Margin of the Ordos Basin, NW China. *Pet. Exploration Dev.* 47 (3), 5–16. (in Chinese, English abstract). doi:10.1016/s1876-3804(20)60066-0
- Li, Y. J., Li, X. Y., and Wang, Y. L. (2015). Effects of Composition and Pore Structure on the Reservoir Gas Capacity of Carboniferous Shale from Qaidam Basin, China. *Mar. Pet. Geology.* 62, 44–57. doi:10.1016/j.marpetgeo.2015.01.011
- Li, Y., Zhang, T., Ellis, G. S., and Shao, D. (2017). Depositional Environment and Organic Matter Accumulation of Upper Ordovician-Lower Silurian marine Shale in the Upper Yangtze Platform, South China. *Palaeogeogr. Palaeoclimatol. Palaeoecol.* 466, 252–264. doi:10.1016/j.palaeo.2016.11.037
- Liu, C. L., Zhang, X., and Yang, Y. Y. (2016). Carboniferous Shale Gas System Evaluation for the Delingha Depression in Qaidam Basin. *Earth Sci. Front.* 23 (5), 135–145. (in Chinese, English abstract). doi:10.13745/j.esf.2016.05.015
- Liu, Q., Li, P., Jin, Z., Liang, X., Zhu, D., Wu, X., et al. (2021). Preservation of Organic Matter in Shale Linked to Bacterial Sulfate Reduction (BSR) and Volcanic Activity under marine and Lacustrine Depositional Environments. *Mar. Pet. Geology.* 127, 104950. doi:10.1016/j.marpetgeo.2021.104950
- Liu, S. M., Tang, S. H., and Huo, T. (2020). Pore Structure and Fractal Characteristics of the Upper Carboniferous Shale, Eastern Qaidam Basin. *Nat. Gas Geosci.* 31 (8), 1069–1081. (in Chinese, English abstract). doi:10.11764/j.issn.1672-1926.2020.02.003
- Loucks, R. G., Reed, R. M., Ruppel, S. C., and Hammes, U. (2012). Spectrum of Pore Types and Networks in Mudrocks and a Descriptive Classification for Matrix-Related Mudrock Pores. *Bulletin* 96, 1071–1098. doi:10.1306/08171111061
- Luo, W., Hou, M., Liu, X., Huang, S., Chao, H., Zhang, R., et al. (2018). Geological and Geochemical Characteristics of marine-continental Transitional Shale from the Upper Permian Longtan Formation, Northwestern Guizhou, China. *Mar. Pet. Geology.* 89, 58–67. doi:10.1016/j.marpetgeo.2017.06.029
- Ng, C., Vega, C. S., and Maranhão, M. d. S. A. S. (2019). Mixed Carbonate-Siliciclastic Microfacies from Permian Deposits of Western Gondwana: Evidence of Gradual marine to continental Transition or Episodes of marine Transgression? *Sediment. Geology.* 390, 62–82. doi:10.1016/j.sedgeo.2019.07.006
- Qi, K. N., Peng, B., and Li, Z. X. (2018). The Characteristics of Reservoir and Control Factors of Clastic Rock of Upper Carboniferous Keluke Formation in Eastern Qaidam Basin. *Geol. Rev.* 64 (5), 1263–1276. (in Chinese, English abstract). doi:10.16509/j.georeview.2018.05.017
- Qi, Y., Ju, Y., Tan, J., Bowen, L., Cai, C., Yu, K., et al. (2020). Organic Matter Provenance and Depositional Environment of marine-to-continental Mudstones and Coals in Eastern Ordos Basin, China-Evidence from Molecular Geochemistry and Petrology. *Int. J. Coal Geology.* 217, 103345. doi:10.1016/j.coal.2019.103345
- Silva, R. O., Leite, M. G. P., Rudnitzki, I., and Souza-Lima, W. (2021). Permian Mixed Carbonate-Siliciclastic Lagoon Coastal System in West-Central Gondwana. *Sediment. Geology.* 414, 105829. doi:10.1016/j.sedgeo.2020.105829
- Song, D. J., Tuo, J. C., and Wang, Y. T. (2019). Research Advances on Characteristics of Nanopore Structure of Organic-Rich Shales. *Acta Sedimentologica Sinica* 37 (6), 1309–1323. (in Chinese, English abstract). doi:10.14027/j.issn.1000-0550.2019.030
- Sweere, T., van den Boorn, S., Dickson, A. J., and Reichart, G.-J. (2016). Definition of New Trace-Metal Proxies for the Controls on Organic Matter Enrichment in marine Sediments Based on Mn, Co, Mo and Cd Concentrations. *Chem. Geology.* 441, 235–245. doi:10.1016/j.chemgeo.2016.08.028
- Wei, X. J., Ma, Y. S., and Li, Z. X. (2018). High-frequency Alternations and Driving Mechanisms of Clastic-Carbonate Successions in the Upper Carboniferous, Northern Qaidam Basin. *J. Palaeogeogr.* 20 (3), 409–422. (in Chinese, English abstract). doi:10.7605/gdxb.2018.03.030
- Yan, D. Y., Huang, W. H., and Zhang, J. C. (2015). Characteristics of marine-continental Transitional Organic-Rich Shale in the Ordos Basin and its Shale Gas Significance. *Earth Sci. Front.* 22 (6), 197–206. (in Chinese, English abstract). doi:10.13745/j.esf.2015.06.015
- Yang, C., Zhang, J., Tang, X., Ding, J., Zhao, Q., Dang, W., et al. (2017). Comparative Study on Micro-pore Structure of marine, Terrestrial, and Transitional Shales in Key Areas, China. *Int. J. Coal Geology.* 171, 76–92. doi:10.1016/j.coal.2016.12.001
- Yang, Y. F., Rao, D., and Fu, X. D. (2014). Generation Conditions of Shale Gas in Carboniferous Keluke Formation, Northern Qaidam Basin. *Pet. Geology. Exp.* 36 (6), 692–697. (in Chinese, English abstract). doi:10.11781/sysydz201406692
- Yin, A., Rumelhart, P. E., Butler, R., Cowgill, E., Harrison, T. M., Foster, D. A., et al. (2002). Tectonic History of the Altyn Tagh Fault System in Northern Tibet Inferred from Cenozoic Sedimentation. *Geol. Soc. America Bull.* 114, 1257–1295. doi:10.1130/0016-7606(2002)114<1257:thotat>2.0.co;2
- Yin, A., Dang, Y. Q., and Wang, L. C. (2008). Cenozoic Tectonic Evolution of Qaidam basin and its Surrounding Regions (Part I): The Southern Qilian Shan-Nan Shan Thrust belt and Northern Qaidam basin. *GSA Bull.* 120 (7/8), 813–846. doi:10.1130/b26180.1

- Zecchin, M., and Catuneanu, O. (2017). High-resolution Sequence Stratigraphy of Clastic Shelves VI: Mixed Siliciclastic-Carbonate Systems. *Mar. Pet. Geology*. 88, 712–723. doi:10.1016/j.marpetgeo.2017.09.012
- Zhang, J. Z., Li, X. Q., and Wang, Y. (2015). Accumulation Conditions and Reservoir Characteristics of marine-terrigenous Facies Coal Measures Shale Gas from Longtan Formation in South Sichuan Basin. *J. China Coal Soc.* 40 (8), 1871–1878. (in Chinese, English abstract). doi:10.13225/j.cnki.jccs.2015.0320
- Zhang, Y., Chen, S. Y., and Sun, J. P. (2016). Lithofacies and Sedimentary Environment of Shale in Carboniferous Keluke Formation, Northern Qaidam Basin. *Earth Sci. Front.* 23 (5), 86–94. (in Chinese, English abstract). doi:10.13745/j.esf.2016.05.009
- Zhang, W., Jian, X., Fu, L., Feng, F., and Guan, P. (2018). Reservoir Characterization and Hydrocarbon Accumulation in Late Cenozoic Lacustrine Mixed Carbonate-Siliciclastic fine-grained Deposits of the Northwestern Qaidam basin, NW China. *Mar. Pet. Geology*. 98, 675–686. doi:10.1016/j.marpetgeo.2018.09.008
- Zhang, L., Dong, D., Qiu, Z., Wu, C., Zhang, Q., Wang, Y., et al. (2021). Sedimentology and Geochemistry of Carboniferous-Permian marine-continental Transitional Shales in the Eastern Ordos Basin, North China. *Palaeogeogr. Palaeoclimatol. Palaeoecol.* 571 (1–3), 110389. doi:10.1016/j.palaeo.2021.110389
- Zou, C., Zhu, R., Chen, Z.-Q., Ogg, J. G., Wu, S., Dong, D., et al. (2019). Organic-matter-rich Shales of China. *Earth-Science Rev.* 189, 51–78. doi:10.1016/j.earscirev.2018.12.002

**Conflict of Interest:** The authors declare that the research was conducted in the absence of any commercial or financial relationships that could be construed as a potential conflict of interest.

**Publisher's Note:** All claims expressed in this article are solely those of the authors and do not necessarily represent those of their affiliated organizations, or those of the publisher, the editors and the reviewers. Any product that may be evaluated in this article, or claim that may be made by its manufacturer, is not guaranteed or endorsed by the publisher.

Copyright © 2022 Guo, Fang, Wang and Wang. This is an open-access article distributed under the terms of the Creative Commons Attribution License (CC BY). The use, distribution or reproduction in other forums is permitted, provided the original author(s) and the copyright owner(s) are credited and that the original publication in this journal is cited, in accordance with accepted academic practice. No use, distribution or reproduction is permitted which does not comply with these terms.